International Journal of Pharmaceutics 676 (2025) 125592

Contents lists available at ScienceDirect

International Journal of Pharmaceutics

journal homepage: www.elsevier.com/locate/ijpharm

Chitosan-aloe vera scaffolds with tuned extracellular vesicles and histatin-5 display osteogenic and anti-biofilm activities☆

Patricia García-García [a,b], Carmen Évora [a,b], Araceli Delgado [a,b,*], Patricia Diaz-Rodriguez [b,c,*]

[a] Department of Chemical Engineering and Pharmaceutical Technology, Universidad de La Laguna 38206 La Laguna, Spain
[b] Institute of Biomedical Technologies (ITB), Universidad de La Laguna 38320 La Laguna, Spain
[c] Department of Pharmacology, Pharmacy and Pharmaceutical Technology, I+D Farma Group (GI-1645), Facultad de Farmacia, Instituto de Materiales (iMATUS) and Health Research Institute of Santiago de Compostela (IDIS), Universidade de Santiago de Compostela 15782 Santiago de Compostela, Spain

ARTICLE INFO

Keywords:
Aloe vera
Chitosan scaffolds
Extracellular vesicles
Bacteria biofilm
Histatin 5

ABSTRACT

The use of extracellular vesicles (EVs) has garnered significant attention as an alternative to cell-based therapies due to their stability and biocompatibility. In this study, we stimulated mesenchymal stem cells (MSCs) with therapeutic agents affecting the bone regenerative cascade, including bone morphogenetic protein 2 (BMP-2), stromal-derived factor (SDF-1), interleukin 4 (IL-4), alendronate (ALD) and osteogenic differentiation media to obtain osteogenic EVs. The tuned EVs were tested on MSCs and fibroblasts, selecting EVs-BMP-2 as suitable systems. Chitosan-aloe vera (AV) scaffolds were designed to allow for the loading and release of these EVs while leveraging the antibacterial and anti-inflammatory properties of AV. To enhance the dual effect on regeneration and antibacterial activity, poly(lactic-co-glycolic acid) (PLGA) microspheres encapsulating Histatin 5 (Hist-5) were incorporated to the scaffolds. Hist-5 encapsulation was successful, and effectively prevented *Staphylococcus aureus* biofilm formation on the scaffolds surface. The optimized chitosan-AV scaffolds loaded with EVs-BMP-2 promoted MSCs adhesion and proliferation and exhibited a 2-fold increase in osteogenic differentiation compared to chitosan scaffolds. This study demonstrates the successful combination of bioengineered EVs and Hist-5-loaded microspheres within a chitosan-AV scaffold, providing a promising dual approach for enhancing bone regeneration while reducing the risk of infection. These systems show potential as effective implants for bone fractures, offering both antibacterial and regenerative capabilities.

1. Introduction

Bone tissue undergoes constant remodeling throughout life. This complex physiological process involves cells, soluble factors and extracellular matrix (ECM) changes. Bone injuries can be self-repaired without external intervention. Nevertheless, when high mass loss takes place, this capacity is overwhelmed requiring surgical intervention and the use of natural or artificial grafts as biomaterials (Pape et al., 2010). Moreover, aging and the occurrence of pathologies such as diabetes and osteoporosis can lead to bone regeneration impairment. In these situations, implants or fillers are necessary to provide structural support and guidance to induce new bone formation (Zhang et al., 2024).

Extracellular vesicles (EVs) are nanometric lipid bilayer structures secreted by various cell types such as mesenchymal stem cells, osteoblasts and osteoclasts among others. EVs present low immunogenicity and are mediators of various tissue homeostasis processes thank to their high cell and tissue penetration capacity (Koritzinsky et al., 2017). EVs secreted by osteoclasts, main actors in bone resorption, have been reported to decrease osteoblast activity while inducing osteoclastogenesis. On the other hand, osteoblast, drivers of bone formation, secrete EVs with proven osteogenic capacity. Finally, mesenchymal stem cells (MSCs)-derived EVs have shown pro-osteoblastic and angiogenic features together with a decreased ECM remodeling response. Overall, these structures play a crucial role in controlling bone homeostasis and could induce regeneration by modulating the differentiation and

☆ This article is part of a special issue entitled: 'Parenteral Time-Controlled Drug Delivery' published in International Journal of Pharmaceutics.

* Corresponding authors at: Institute of Biomedical Technologies (ITB), Universidad de La Laguna, 38320 La Laguna, Spain (Araceli Delgado). Department of Pharmacology, Pharmacy and Pharmaceutical Technology, I+D Farma Group (GI-1645), Facultad de Farmacia, Instituto de Materiales (iMATUS) and Health Research Institute of Santiago de Compostela (IDIS), Universidade de Santiago de Compostela 15782 Santiago de Compostela, Spain (Patricia Diaz-Rodriguez).
E-mail addresses: adelgado@ull.edu.es (A. Delgado), patricia.diaz.rodriguez@usc.es (P. Diaz-Rodriguez).

https://doi.org/10.1016/j.ijpharm.2025.125592
Received 30 December 2024; Received in revised form 5 April 2025; Accepted 11 April 2025
Available online 12 April 2025
0378-5173/© 2025 The Authors. Published by Elsevier B.V. This is an open access article under the CC BY-NC license (http://creativecommons.org/licenses/by-nc/4.0/).

function of the cells implicated in the process (Gao et al., 2018; Man et al., 2023; Mehrvar et al., 2024; Ren et al., 2022; Tang et al., 2024).

Although EVs are released spontaneously by cells, the modulation of their cargo by either stimulating the parental cells or artificially inserting molecules before or after EVs synthesis, has been proposed to enhance their therapeutic potential (Lu et al., 2023). The first approach is based on the capacity of the stimulating factor to induce changes in the cell's phenotype leading to concomitant variations in the EVs cargo. In this regard, the stimulation of MSCs with different cytokines and chemical moieties as metformin or kartogenin have been proven to modify the chondrogenic and immunomodulatory capacity of the derived EVs (Chen et al., 2022).

Despite the huge therapeutic potential of EVs their systemic administration leads to limited accumulation at the target site. Therefore, the development of systems able to release the therapeutic vesicles at the desired place represents an alternative approach to better take advantage of their therapeutic ability. In this regard, biomaterials encompassing MSCs-EVs have been already described in the literature to depict improved osteogenic and angiogenic responses in preclinical rodent models when compared to non-loaded scaffolds. Different types of biomaterials have been screened for these purposes as scaffolds based on metals (titanium alloys), ceramics (tricalcium phosphate, mesoporous bioactive glass) and polymers (PLGA, PLGA-PEG-PLGA) or injectable hydrogels of hyaluronic acid/alginate/hydroxyapatite, gelatin methacrylate and hydroxyapatite/silk fibroin/glycol chitosan/difunctionalized polyethylene glycol (He et al., 2024; Lu et al., 2023; Ren et al., 2022; Yang et al., 2020; Youseflee et al., 2023). However, mainly non-bioengineered MSC-EVs have been screened for this purpose.

Chitosan is a natural polymer with antibacterial, antioxidant and anti-inflammatory properties (Aranaz et al., 2021; Garcia-Garcia et al., 2021). It is a polycation polysaccharide due to the presence of amine groups that confer positive charges at acidic pHs. This property could induce the immobilization of EVs by electrostatic interactions based on their negative surface charge allowing for EVs sustained release (Man et al., 2022; Zhang et al., 2018). As already reported by our research group, chitosan scaffolds can be obtained by a molding-freeze drying method that leads to the fabrication of highly porous structures, suitable for cell adhesion and proliferation (Garcia-Garcia et al., 2021; Reyes et al., 2012). This feature would also facilitate EVs adsorption into the scaffold surface.

The surgical interventions required for bone fracture management entail the risk of osteomyelitis. These procedures involve open surgery and usually drilling and cleaning steps leading to the surrounding tissue necrosis. Under this stressed environment, osteocytes lose their inhibitory activity on osteoclast, increasing osteoclast activity and compromising immunity generating a susceptible infection site (Jensen et al., 2017; Shiels et al., 2015). Bone infections are a major burden for health care systems, with an annual prevalence of approximately 21.8 cases per 100,000 people. Furthermore, they are complex to eradicate due to the low bone antibiotic accumulation (De Oliveira et al., 2020; Kremers et al., 2015). *Staphylococcus aureus* (*S. aureus*), included in the ESKAPE group, is one of the main pathogens causing bone infections. This group of multiple-drug resistant pathogens can attach to bone implants and fillers forming biofilms. These structures comprised of a self-produced extracellular matrix, hinder even more the penetration of antibiotics to the infection site (Moormeier and Bayles, 2017).

The fight against antimicrobial resistance (AMR) is one of the most pressing needs of the twenty-first century. Currently, resistant bacteria kill 700,000 people in the world every year, and this number is expected to increase to 1 million by 2050 (Tarin-Pello et al., 2022; Wang et al., 2023). The misuse of antibiotics together with the lack of new antibiotics in the last 50 years has led to an enhancement of resistant bacteria. Therefore, alternatives to antibiotics are required to avoid the growth of AMR. Moreover, an adequate release profile is required to ensure the long-term activity of these alternatives. This issue can be addressed by their incorporation in drug delivery systems like microspheres or hydrogels. Antimicrobial peptides are small molecules naturally produced by organisms representing their first line of defense against bacteria, viruses and fungi (Boparai and Sharma, 2020). Among them, histatin 5, a histidine-rich cationic peptide identified in the saliva of humans and higher primates, stands out by its high antifungal and bactericidal activity against ESKAPE pathogens. At 30 μM histatin 5 kills 70 % of *S. aureus* after 5 h of contact (Du et al., 2017). Another family of well-known antimicrobial biomolecules are phytochemicals. *Aloe barbarensis Miller*, commonly named aloe vera, is a plant member of the Liliaceae family. Its phytochemicals have been associated with numerous properties, such as anti-inflammatory, antimicrobial, osteogenic, anti-arthritic and pro-healing (Hashemi et al., 2015; Radha and Laxmipriya, 2015). The extracts obtained from aloe vera contains approximately 75 active compounds, of which anthraquinones and polysaccharides show antimicrobial properties against Gram-positive and Gram-negative bacteria, including *S. aureus* (Gomez Chabala et al., 2017; Habeeb et al., 2007; Hamman, 2008).

The present study aims at developing chitosan-based advanced scaffolds comprising biodegradable microspheres able to induce bone formation while avoiding osteomyelitis. To this end, pro-osteogenic MSC-EVs and an aloe vera extract will be incorporated to the chitosan network whereas histatin-5 will be incorporated within the microspheres to allow for a controlled release. Pro-osteogenic EVs will be obtained by stimulating MSCs with molecules known to control bone homeostasis (Interleukin-4 (IL-4); Bone Morphogenetic Protein-2 (BMP-2); Alendronate (ALD) osteogenic media and stromal cell derived factor 1 (SDF-1)). To the best of our knowledge, this work combines, for the first time, tuned MSCs-EVs with alternatives to antimicrobials with dual release profiles for bone regeneration.

2. Materials and methods

2.1. Materials

Poly (lactic-co-glycolic acid) (PLGA) 50:50 (Resomer® RG504) and PLGA 85:15 (Resomer® RG858-S) were supplied by Evonik Industries (Germany). Chitosan hydrochloride (Protasan® UP-CL-213) was purchased from NovaMatrix (Norway). Cell proliferation kit II (XTT) was purchased from Roche Diagnostics (Germany). Dulbecco's modified Eagle's medium (DMEM) and Dulbecco's phosphate buffered saline (DPBS) were obtained from Gibco. Fetal bovine serum (FBS) was purchased from Lonza (Spain). Poly (vinyl alcohol) (PVA, MW 33,000–70,000 Da; 87 – 90 % hydrolyzation), sodium triphosphate pentabasic (TPP, MW: 367.86 g/mol), penicillin/streptomycin, L-glutamine, dexamethasone (MW: 392.46), sodium lauryl sulfate (SDS, MW: 288.38 g/mol) and β-glycerol 2-phosphate disodium salt hydrate (MW:216.04 g/mol) were supplied by Sigma-Aldrich, USA. L-Ascorbic acid (MW: 176.13) was purchased from Acofarma, Spain. Nitroblue Tetrazolium (NBT) and 5-bromo-4-chloro-3-indolyl phosphate (BCIP) were purchase from Roche Diagnostics, Germany. Calcium chloride ($CaCl_2$) and monobasic sodium phosphate dihydrate was provided by Merck, Germany. Mueller-Hinton Agar was purchased from Applichem Panreac, Germany. Histatin 5 (Hist-5; H-DSHAKRHH-GYKRKFHHSHRGY-OH) was provided by Eurogentec, USA. Recombinant mouse SDF-1 alpha protein was purchased from Abcam (ab51939), USA. Human bone morphogenetic protein-2 (BMP-2) was obtained from GenScript, USA and recombinant Human Interleukin 4 (IL-4) was purchased from Gibco, Thermo Fisher Scientific, USA. Aloe vera extract (AV) was supplied by Agora Valencia, Spain.

2.2. Mscs stimulation, EVs isolation and characterization

Extracellular vesicles (EVs) were isolated from murine mesenchymal stem cells (MSCs, C3H10T1/2; ATCC CCL-226). To obtain tuned EVs, MSCs were stimulated with several inductors before isolation. Cells were cultured with DMEM supplemented with 10 % FBS, 1 % penicillin/

streptomycin and 1 % L-glutamine (complete DMEM) at 37 °C and 5 % CO_2 until 80 % confluence was obtained. Then, cell monolayers were treated with the selected molecules for the required time as described in Table 1. After stimulation, cell monolayers were washed with DPBS and EVs isolation medium was added. This medium was composed by DMEM + 1 % penicillin/streptomycin + 1 % L-glutamine + 5 % EVs-free FBS (obtained by ultrafiltration as previously reported) (Briffault et al., 2024). Cells were then maintained for 48 h in culture and EVs were isolated by ultracentrifugation as previously described (Briffault et al., 2024). Briefly, cell supernatants were centrifuged consecutively at 2,000 g and 4 °C for 30 min to remove dead cells, afterwards at 10,000 g and 4 °C for 30 min to discard cell debris and, finally, at 100,000 g and 4 °C for 2 h to precipitate EVs. The obtained pellet was resuspended in 1 mL DPBS per flask (75 cm^2) and filtered through 0.22 μm (PES membranes Millex®, Millipore, UK).

Cell stimulation was performed using different molecules with already known activities in the bone remodeling process: sodium alendronate (ALD, 10 μg/mL), interleukin 4 (IL-4, 20 ng/mL), stromal cell-derived factor 1 (SDF-1, 500 ng/mL), bone morphogenetic protein 2 (BMP-2, 200 ng/mL) and osteogenic differentiation medium (DF). Osteogenic medium (DF) was composed by complete media supplemented with 10 mM β-glycerol phosphate, 10^{-7} M dexamethasone and 50 μM ascorbic acid (Jaiswal et al., 1997). The stimulation with osteogenic media was performed for 72 h instead of 24 h. Furthermore, an additional BMP-2 stimulation condition was included incorporating the protein at 200 ng/mL to the EVs isolation media. All the conditions used are summarized in Table 1.

After isolation EVs were characterized in terms of particle size, polydispersity index (PdI), and zeta-potential (ζ-potential) using a Zetasizer Nano-ZS (Malvern Instruments, UK). To this end, samples were 1:10 diluted with DPBS and measurements were performed in triplicate.

Additionally, the EVs-associated protein was measured using a Micro BCA Protein Assay Kit (Thermo Fisher Scientific, USA). For this purpose, vesicles were lysed by appropriate dilution with 0.2 % SDS in DPBS (Vergauwen et al., 2017) and subsequently subjected to 6 cycles of sonication for 30 s at 30 s intervals.

2.3. Effect of tuned EVs on cell viability and proliferation

The effect of the different chemically conditioned EVs on cell proliferation was studied in MSCs and murine fibroblasts (BALB 3 T3, ATCC). Cells were seeded in 96-well plates at 10,000 cells/well for MSCs or 15,000 cells/well for fibroblasts and allowed to attach for 24 h. Cell monolayers were then washed with 200 μL of DPBS and, afterwards, 200 μL of isolation medium supplemented with 10 % of EVs suspension was added. Cells were kept in culture for 96 h. After this time, cell monolayers were washed twice with 200 μL DPBS and a XTT assay was performed following the manufacturer's instructions to quantify cell proliferation. Then, absorbance was measured in a plate reader (synergy HT, BioTek, USA) at 450 nm. Isolation media with 10 % DPBS was used as control.

Table 1
Conditions used for the isolation of bioengineered EVs.

Chemical stimulus	*Dose*	*Stimulation time*
BMP-2	200 ng/mL	24 h before EVs isolation
SDF-1	500 ng/mL	24 h before EVs isolation
IL-4	20 ng/mL	24 h before EVs isolation
ALD	10 μg/mL	24 h before EVs isolation
DF	–	72 h before EVs isolation
DF + ALD	10 μg/mL ALD	72 h in presence of DF + 24 h in contact with ALD before EVs isolation
BMP-2 after	200 ng/mL	48 h, during EVs isolation

2.4. Microspheres preparation and characterization

Histatin 5 (Hist-5) microspheres were prepared by a double emulsion (w/o/w) solvent evaporation method as previously described (Garcia-Garcia et al., 2019). Briefly, 200 μL of a 0.2 % PVA aqueous solution containing 2 mg of Hist-5 was emulsified with 1 mL of methylene chloride (DCM) containing 150 mg/mL PLGA (PLGA 504: PLGA 858-S (80:20)), using a vortex for 1 min (position 10, Genie® Industries 2, Sciences Industries Inc. USA). Then, 5 mL of 0.2 % PVA were added to the emulsion and vortexed for 15 s. Immediately, the emulsion was poured into 100 mL of 0.1 % PVA under magnetic stirring for 1 h to evaporate the DCM. After this time, the microspheres were isolated through filtration (PES membrane, Pall Corporation, pore size 45 μm, Sigma-Aldrich, USA), freeze dried and stored at 4 °C until use.

To determine the microspheres encapsulation efficiency, Hist-5 was labeled with ^{125}INa (Perkin-Elmer) following the previously described iodogen method (Del Rosario et al., 2015). Briefly, 50 μL of a phosphate buffer (PB, 0.5 M, pH = 7), 50 μL of Hist-5 (5 μg/ μL) and 1 μL of ^{125}INa (0.1 mCi) were added to a precoated Iodination Tube (Thermo Scientific, USA). This mixture was subjected to orbital agitation at 125 rpm for 10 min at room temperature. ^{125}I-Hist-5 radiolabeling efficiency was determined by thin layer chromatography (iTLC) using 11.5x0.8 cm silica-gel coated strips (Varian Iberica SL). ^{125}I-Hist-5 was diluted (1:500 in MilliQ water) and 5 μL of the dilution (approximately 30.000–40.000 cpm) was loaded onto the chromatography strip, chromatography was performed using MeOH:H_2O (85:15) as mobile phase. The free ^{125}I migrates to the front (Rf = 1) while the labeled product remains on the base (Rf = 0). When the mobile phase reached the top, the chromatography paper was removed, cut by half and radioactivity measured on a gamma counter (Cobra II, Packard). The radiolabeling efficiency was calculated from the ratio between the radioactivity at the base (Rf = 0) and the total radioactivity (Rf = 0 + Rf = 1). On the other hand, the microspheres ^{125}I-Hist-5 encapsulation efficiency was determined by measuring the radioactivity of known weights of microspheres (approximately 5 mg) using a gamma counter. The encapsulation efficiency was calculated from the ratio of the measured radioactivity to the total radioactivity used in the batch preparation, both normalized by product weight.

Microspheres morphology was analyzed by scanning electron microscopy (SEM, ZEISS EVO 15, Tokio, Japan). For this purpose, samples were coated with gold before observation. Microspheres size distribution was determined by laser diffractometry using a Mastersizer 2000 (Malvern Instruments, Malvern, UK). Samples were resuspended in water under continuous flow to perform the measurements.

2.5. In vitro antibacterial activity of Hist-5

The antibacterial activity was determined against *Staphylococcus aureus* (ATCC 25293; gently donated by Department of Biochemistry, Microbiology, Cellular Biology and Genetics of the University of La Laguna). *Staphylococcus aureus* was routinely cultured in Mueller-Hinton Agar at 37 °C. After 24 h, one colony forming unit (CFU) was seeded in 25 mL of nutrient broth and incubated for 18 h at 37 °C under orbital shaking (150 rpm). Then, the bacterial suspension was centrifuged at 2,000 g for 12 min, the nutrient broth was removed, and the bacterial pellet was washed three times with a mixture of nutrient broth and Phosphate Buffer10 mM, pH 7.4 (PB) (1:10) (bacterial working medium) using the same centrifugal conditions. Bacteria pellet was resuspended in bacterial working medium to obtain a suspension with a 0.5 McFarland turbidity (1.5 x 10^8 CFU/mL). Subsequently, the bacterial suspension was added to 24-well plates (500 μL per well). Then, 100 μL of Hist-5 solutions at different concentrations (1.62—0.06 μg/μL) were added to each well and incubated at 37 °C under orbital shaking for 6 h. After this time, each bacterial suspension was diluted with MilliQ water and 20 μL were pipetted in Muller Hinton agar plates by triplicate. The agar plates were incubated at 37 °C for 24 h and the total number of CFU was afterwards counted for each plate.

2.6. Scaffold preparation and characterization

2.6.1. Scaffold preparation

To prepare four-millimeter diameter chitosan scaffolds (CHT), 12 mg microspheres (2 mg of blank microspheres and 10 mg of Hist-5 microspheres) were dispersed in 40 μL of a chitosan dispersion at 2 % (w/v) and freeze dried. The scaffolds were then cross-linked with 40 μL of 5 % (w/v) sodium tripolyphosphate (TPP) for 3 min, washed twice with 80 μL of MilliQ water and freeze dried again. For CHT scaffolds containing aloe vera extract (AV), two additional steps were performed. After the second freeze drying, 13.5 μL of an aqueous suspension of the extract containing 2, 4 or 8 mg the solid extract (CHT-AV2, CHT-AV4 and CHT-AV8) were added to each scaffold and freeze dried. Then, 20 μL of 70 % ethanol was added to each scaffold and kept in an extraction hood for 1 h to facilitate solvent evaporation, the obtained systems were then immediately freeze dried. Scaffolds were characterized in terms of porosity, water uptake, and mass loss. The morphology of either fresh scaffolds or systems subjected to 7 days soaking in water at 37 °C were observed by SEM (ZEISS EVO 15, Tokio, Japan) after gold coating.

2.6.2. Water uptake and mass loss

Scaffolds' porosity was calculated using the Eq. (1), where ρ_{app} and ρ_{real} are the apparent and real density, respectively. The apparent density was calculated by dividing the mass by the geometric volume of the system (height x width x thickness). On the other hand, the real density was measured using a helium pycnometer (AccuPyc 1330, Micromeritics, USA).

$$Porosity(\%) = \left(\frac{\rho_{real} - \rho_{app}}{\rho_{real}}\right)x100 \quad (1)$$

Scaffolds' water uptake and mass loss studies were carried out by incubating them in water at 37 °C. At different timepoints, three samples were taken, excess water was removed using filter paper, scaffolds were weighed and freeze dried to obtain the final dry weight. Water uptake and mass loss were calculated using Eqs. (2) and (3), respectively. Where W_o is the initial weight of each system, W_w is the wet weight, and W_d is the final weight after freeze drying.

$$Wateruptake(\%) = \left(\frac{W_0 - W_d}{W_0}\right)x100 \quad (2)$$

$$Massloss(\%) = \left(\frac{W_w - W_d}{W_d}\right)x100 \quad (3)$$

The release of AV from the scaffolds was evaluated by spectrophotometry. An AV calibration curve between 2—0.25 mg/mL was prepared and the absorbance was measured at 254 nm (Ultrospect 3300 pro, Biochrom, UK). Scaffolds were placed in 2 mL of MilliQ water at 37 °C and, at different timepoints (0,25, 1, 2, 5 and 7 days), three scaffolds were removed, and the absorbance of the supernatants were measured.

2.6.3. Extracellular vesicles loading and release assay

Scaffolds were loaded with the EVs taking advantage of the interactions between the cationic chitosan and the negatively charged EVs surface caused by the presence of sialic acid residues. This was achieved by pipetting 40 μL of EVs suspension onto the chitosan scaffolds followed by a 30 min incubation. The release of EVs from the CHT scaffolds was studied using a Micro BCA Protein Assay Kit (Thermo Fisher Scientific, USA). DPBS (360 μL) was added as release medium to the loaded scaffolds and incubated at 37 °C. Release media samples were collected at different timepoints and the EVs content was determined using the MicroBCA kit following the manufacturer's instructions. The amount of EVs released immediately after DPBS addition was considered as free-EVs and used to determine the loading efficiency.

2.6.4. Scaffolds antimicrobial activity

The antimicrobial activity of the scaffolds containing blank microspheres and either chitosan alone (CHT) or chitosan and aloe vera extract at different amounts (CHT-AV2, CHT-AV4 and CHT-AV8) was studied using an agar diffusion test. Bacterial suspensions, prepared as described in section 2.5, were diluted to an optical density of 0.5 McFarland and seeded using cotton swabs on Mueller Hinton agar plates. Then, scaffolds were placed on top of the seeded plates and 40 μL of PB were dropped on the scaffolds' surface, plates were then incubated at 37 °C. After 24 h of incubation, pictures of the culture plates were taken and the normalized inhibition width (nw) was determined following Eq. (4) (Marti et al., 2018):

$$nw = \frac{\frac{di-d}{2}}{d} \quad (4)$$

Where d is the diameter of the scaffolds and di is the diameter of inhibition zone.

2.6.5. Antibiofilm activity of the developed scaffolds

The antibiofilm activity of CHT and CHT-AV2 scaffolds with and without Hist-5 microspheres against *S. aureus* was assessed using the Amsterdam Active Attachment (AAA) biofilm model as previously described with slight modifications (Vivero-Lopez et al., 2021). The designed model was based on a surgical grade stainless steel sheet containing needles working as a lid for a 24-well plate (Fig. 1). Bacterial suspensions at 8 ± 2.5 CFUx10^6/mL in the bacterial working medium were placed on the 24-well plate (600 μL per well). Afterwards, the scaffolds were punched in the needles and held in place with silicone pieces. The lid was then placed closing the well plate and leading to the immersion of the scaffolds in the bacterial suspension. Scaffolds were incubated for 24 h at 37 °C, removed from the bacterial suspension and washed with 600 μL of 10 mM PB to remove bacteria not incorporated within the biofilm. Afterwards, the biofilm formed was disrupted by adding 400 μL of bacterial working medium and shaken vigorously for 15 min. Additionally, the growth capacity of biofilm-entrapped bacteria was assessed by keeping the scaffolds on the AAA support and transferring them, after PB washing, to complete culture broth for another 24 h. In both cases the bacterial viability was assessed by XTT mixing 150 μL of the bacterial supernatant with 50 μL of the XTT reagent mixture and allowing for a 2-hour incubation. To quantify the bacterial concentration a calibration curve using an XTT was prepared between 2 CFUx10^6/mL and 16 CFUx10^6/mL. Round glass coverslips were used as positive control (Thermo Scientific, USA). To avoid contact with the bottom of the plate, coverslips were placed between two pieces of 1x2 mm silicone.

2.7. In vitro biological performance of chitosan scaffolds

2.7.1. Cell viability, adhesion and proliferation

Chitosan scaffolds prepared with blank microspheres with or without AV (CHT, CHT-AV2, CHT-AV4 and CHT-AV8) and with or without EVs-BMP-2, were used to evaluate MSCs adhesion and proliferation. EVs-BMP-2 (2.34x10^8 particles/mL) were loaded as previously described (section 2.6.3). Scaffolds were placed on non-adherent plates, seeded with 40 μL of a cell suspension at 1.25 10^6 cells/mL and incubated for 1.5 h at 37 °C and 5 % CO_2 to allow cell adhesion. After this time, 360 μL of isolation medium was added. After 12 and 48 h of seeding, cell adhesion and proliferation was assessed by a XTT test following the manufacturer's instructions. To do so, each scaffold was washed twice with 200 μL of DPBS, and then 200 μL of complete DMEM and XTT working reagent (10:1) was added to each well and incubated for 2 h at 37 °C and 5 % CO_2. After this time, absorbance was measured at 445 nm using a plate reader (Biotek, Winooski, USA).

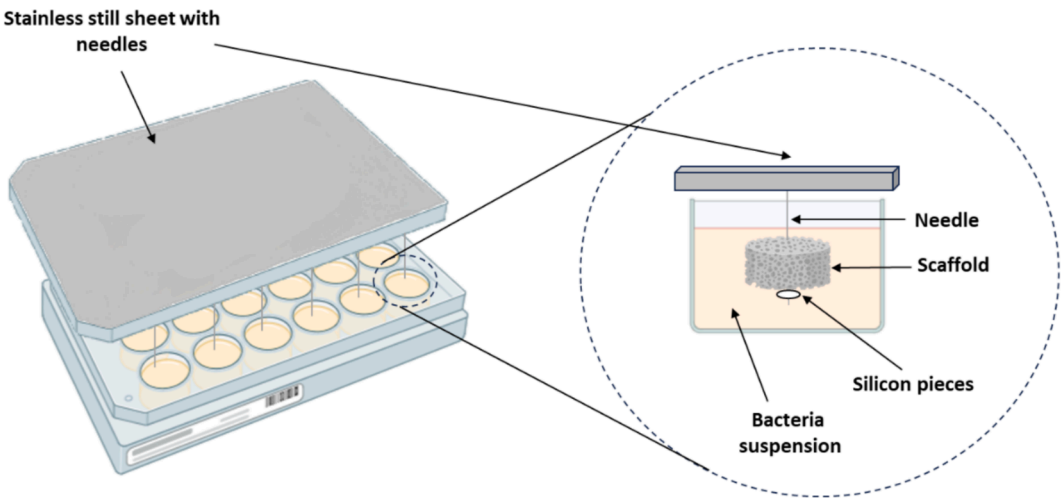

Fig. 1. Amsterdam Active Attachment (AAA) biofilm model setup.

2.7.2. Osteogenic differentiation evaluation

Alkaline phosphatase (ALP) activity was measured to assess the osteogenic induction capacity of the developed scaffolds in MSCs. This assay was performed in CHT and CHT-AV with and without EVs-BMP-2. Cells were seeded on the scaffolds and cultured as previously described (section 2.7.1). After 48 h, media was replaced by complete media for the rest of the assay changing media every other day. At 7, 14, 21 and 28 days, samples were removed, washed twice with DPBS at 4 °C and fixed with buffered 4 % paraformaldehyde (PFA, Panreac, Barcelona) for 30 min. Then scaffolds were washed twice with DPBS again and 400 μL of 0.5 mg/mL nitro-blue tetrazolium chloride (NBT) and 0.18 mg/mL 5-bromo-4-chloro-3-indole phosphate (BCIP) prepared in 0.1 M Tris-HCl, 0.1 M NaCl and 0.05 M $MgCl_2{\cdot}6H_2O$ (pH = 9.2–9.5) were added to the scaffolds. Samples were incubated at 37 °C and 5 % CO_2 for 2 h. Afterwards, scaffolds were washed twice with DPBS and included in OCT (Fisher Scientific, USA) at 4 °C for 24 h. After this time, OCT was replaced with fresh OCT and samples were frozen at −20 °C for 24 h. The mounted samples were cut into 50 μm sections with a cryostat (Epredia, USA). Six sections of each scaffold were observed by light microscopy (LEICA DM4000B, Spain) and 30 photographs were taken with a Leica camera (LEICA DFC300FX, Spain) to quantify the number of ALP + cells.

2.8. Statistical analysis

All experiments were performed at least in triplicate and results expressed as mean ± SD. Statistical analysis was performed using the SPSS.27 software. A one-way analysis of variance (ANOVA) with a post-hoc Dunnet test was carried out. Significance was set at $p < 0.05$.

3. Results and discussion

3.1. Extracellular vesicles, isolation and characterization

The EVs cargo and production yield can be modified by stimulating the parent cells with physical and chemical triggers. The production of modified EVs by the chemical stimulation of the cells is simple and does not require specific equipment (Hahm et al., 2021). In the present work, we tuned EVs to obtain pro-osteogenic vesicles by priming MSCs with different modulators already reported to control bone homeostasis and MSC differentiation; BMP-2, SDF-1, IL-4, ALD and the standard osteogenic differentiation media. The bisphosphonate ALD is an inhibitor of bone resorption and a suppressor of osteoclast activity (Fu et al., 2008). On the other hand, IL-4 is a cytokine with already known anti-inflammatory effect and inhibitor of osteoclastogenesis (Bouchareychas et al., 2020; Zheng et al., 2017) while SDF-1 and BMP-2 are growth factors with osteogenic effect (Ji et al., 2004; Liu et al., 2014; Shea et al., 2003). The EVs isolated after the different treatments showed an homogenous distribution similar sizes and PdI not observing any statistical differences between them (Fig. 2). The obtained vesicles depicted a mean diameter within the 206.5 ± 64.3 – 332.14 ± 132.9 nm range except for EVs-IL-4 which showed a superior size of 427.67 ± 59.2 nm (Fig. 2A). Regarding PdI, all the suspensions showed values below 0.38 excluding EVs-IL-4 that showed a mean value of 0.55. As expected, EVs depicted a negative ζ-potential between −8 and −16 mV not observing statistically significant differences between treatments (Fig. 2B). Moreover, tuned EVs also did not show statistically significant differences with the control group in the amount of EVs-associated protein. The mean concentration of protein obtained for the EVs suspension was 480.6 ± 103.8 μg/mL.

Extracellular vesicles are a heterogeneous group of particles at the nanosize range secreted by cells (Gul et al., 2022). Several methodologies have been screened for EVs characterization presenting all of them advantages and disadvantages. The analysis selected for this work is based on light scattering, an already widely-used technique for EVs analysis. The properties shown by the suspensions fit within the EVs characteristics with a main population at 100 nm (Fig. 2C) (Palmieri et al., 2014). Moreover, no differences in the properties of the EVs were observed between the treatments, similar to already reported for other authors. As an example, EVs isolated for atorvastatin treated bone marrow MSCs showed the same features as those obtained from untreated cells and the same happened for infrapatellar Fat Pad MSCs-derived EVs pretreated with kartogenin (Shao et al., 2021; Yu et al., 2020). Interestingly, in a recent study the pretreatment of rat bone marrow MSCs with BMP-2 did not lead to an enhancement in the EVs-associated protein neither a change in their physicochemical properties compared to control (non-treated MSCs)-EVs in agreement with our findings (He et al., 2024).

The effect of the different EVs on cell proliferation was evaluated on MSCs and fibroblast (Fig. 3). The fibroblasts' proliferative activity was decreased in the presence of EVs-BMP-2 and significantly increased in the presence of EVs-ALD when compared to control (DPBS treated cells). In contrast, MSC proliferative activity decreased in the presence of EVs-ALD and increased in the presence of EVs-IL-4 and EVs-control (Fig. 3). Fibroblasts play a fundamental role in the early formation of the callus after fracture thanks to the production of collagen and growth factors with angiogenic activity (Radomsky et al., 1998). However, an exacerbation of their proliferation can produce a fibrotic matrix that interferes with proper fracture healing (Pakshir and Hinz, 2018). Interestingly, the treatments with EVs-DF, EVs-SDF-1 and EVs-BMP-2 were able to decrease the proliferation of fibroblasts while inducing the proliferation

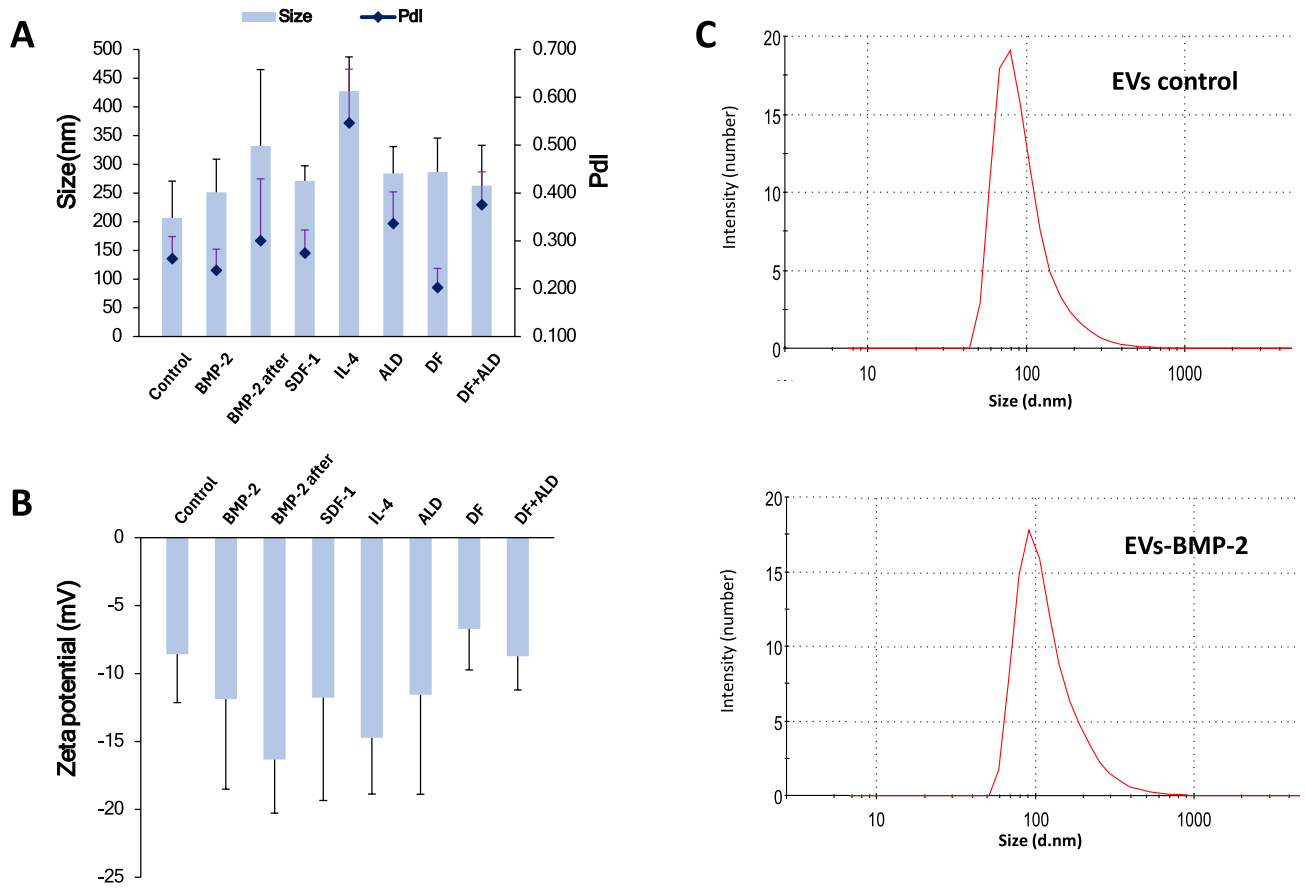

Fig. 2. EVs characterization by DLS to obtain A) Mean hydrodynamic diameter (bars) and PdI (diamonds); B) ζ-potential (bars) and C) size distribution in number. n = 3.

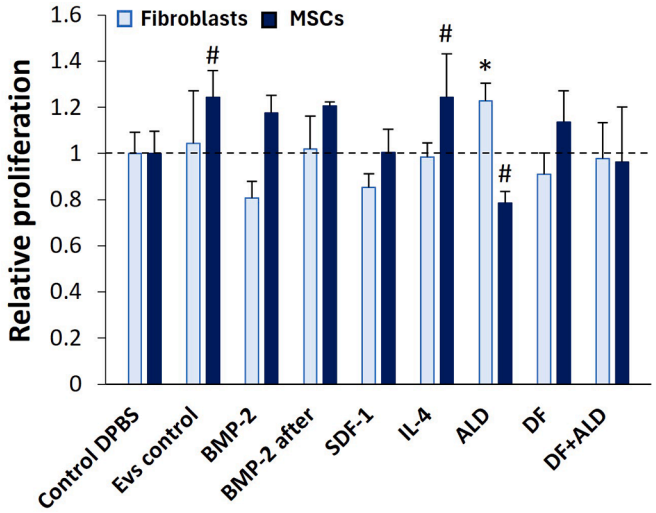

Fig. 3. Relative proliferation, normalized to DPBS treated cells, of fibroblasts and MSCs after 96-hours stimulation with EVs isolated from MSCs pretreated with different conditions. (*) denotes statistical differences to control fibroblasts and (#) denotes statistical differences to control MSCs. $p < 0.05n = 4$.

of MSCs. However, fibroblasts treated with EVs-BMP-2 showed the highest decrease in growth. Based on this, EVs-BMP-2 were selected for further experiments. Remarkably, EVs control, obtained from non-stimulated cells, shows a MSCs proliferation induction. The beneficial effects of MSC-EVs on stem cells proliferation has been previously reported and used as a strategy to promote healing and immune regulation for different applications as osteoarthritis, spinal cord and skin injury, liver, kidney and lung fibrosis (Kou et al., 2022). The osteogenic effect of BMP-2 has been extensively studied in bone fracture regeneration. However, its clinical use has been hampered by limitations such as short half-life, rapid clearance and side effects (Bhakta et al., 2012). The use of EVs obtained from cells previously treated with BMP-2 could allow us to take advantage of the obtained pro-osteogenic environment while avoiding the risk of these undesired side effects.

3.2. Scaffold development and characterization

The mean diameter of blank and Hist-5 loaded microspheres was 90.82 μm (10 % < 52.32 μm; 90 % > 151.70 μm) and 127.68 μm (10 %< 74.26 μm; 90 %> 220.34 μm), respectively. This increase in size could be attributed to the incorporation of the peptide within the polymeric matrix. The incorporation of peptides or therapeutic molecules into PLGA microspheres can influence their size, primarily due to changes in emulsion stability during the fabrication process. These molecules can alter the viscosity and interfacial tension of the emulsion, potentially leading to variations in microsphere size (Martinez-Borrajo et al., 2023; O'Donnell and McGinity, 1997). Microspheres show a monodisperse distribution as shown in Fig. 4A. The encapsulation efficiency of the peptide was 61.62 ± 6.83 % leading to a subsequent loading of 10.6 μg Hist-5/mg. The Hist-5 loaded microspheres were also characterized by Scanning Electron Microscopy images (SEM) showing a smooth round morphology with homogeneous size distribution matching the above-described data and the size distribution (Fig. 4B).

Regarding the physicochemical properties of the scaffolds incorporating the microspheres, systems prepared only with chitosan, CHT, presented a porosity of 86.58 ± 1.27 %. The progressive addition of the

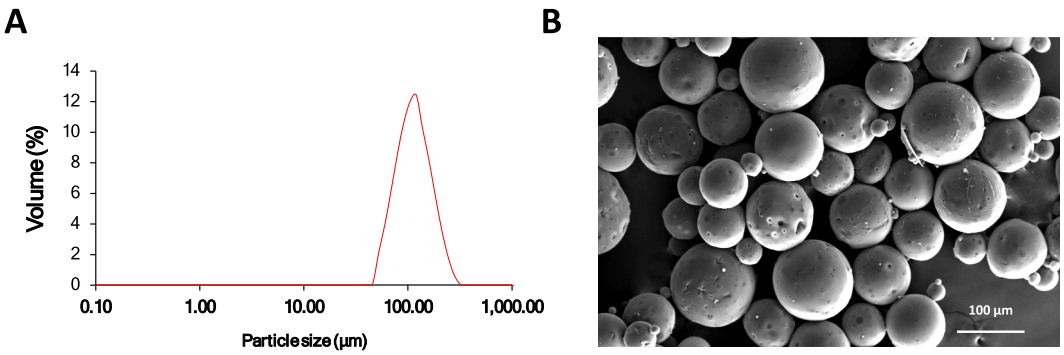

Fig. 4. A) Particle size distribution and B) Scanning Electron Microscopy images of Hist-5 loaded microspheres. Scale bar: 100 µm.

aloe vera extract (AV) to the scaffolds led to a decrease in the porosity from 82.54 ± 0.15 % when 2 mg of aloe vera is added (CHT-AV2) to 78.49 ± 0.87 % when 4 mg of aloe vera are incorporated (CHT-AV4) and 69.75 ± 1.55 % for scaffolds including 8 mg of aloe vera (CHT-AV8). The decrease in porosity could be attributed to both, the incorporation of AV together with the addition of ethanol that could collapse the smaller pores of the scaffold. This phenomenon was previously described for polylactide/chitosan scaffolds (Wan et al., 2007).

The behavior of the scaffolds when immersed in aqueous solution was characterized in terms of water uptake and swelling. The water uptake of CHT scaffolds was higher than that for systems including AV. After 7 days of swelling, the water uptake for CHT was 177.36 ± 7.19 % while CHT-AV2 only showed a water uptake of 101.26 ± 6.8 % (Fig. 5A). The addition of higher amounts of AV to the scaffold did not change the water uptake capacity. That is, scaffolds containing AV do not swell as chitosan scaffolds alone. This lack of water uptake capacity is associated with the porous structure and stability of both types of scaffolds after aqueous immersion. As shown in Fig. 5B, scaffolds comprising AV suffer a higher mass loss at all the studied timepoints. Remarkably, CHT-AV8 systems after just 6 h of soaking in water lost almost half of the weight with an average value of 35.28 ± 4.75 %. This mass loss was stable after this initial timepoint, not observing differences between 6 h and 7 days of soaking. To elucidate whether this weight loss was associated with just the release of AV from the scaffolds, an AV release study was performed. Afterwards, the mass loss associated to AV release was calculated. As shown in Fig. 5B, the loss of mass suffered by the scaffolds was only partially associated with the AV release. Moreover, the release of the AV extract showed a marked burst effect followed by a more sustained release until the end of the study. Aloe vera extract is very water soluble and is released quickly, with a small portion retained within the scaffolds. On the other hand, CHT scaffolds only showed a 10 % mass loss at all the evaluated timepoints indicating a good scaffold integrity after swelling. This is not the case for the scaffolds with AV that not only lose AV mass but also other scaffold components. These results could be related to both, the protocol used for AV incorporation that implies an initial wetting in EtOH, together with a disruption of the scaffold structure. The incorporation of additional components to the chitosan network that do not cross-link within the polymer network can significantly influence the structural and functional properties of the scaffolds. It has been previously reported that the addition of calcium phosphates like hydroxyapatite (HAp) and β-tricalcium phosphate (β-TCP) to chitosan/alginate scaffolds obtained by molding-freeze drying has modified total porosity of the systems (Lopes et al., 2024). A similar behavior was observed for chitosan scaffolds

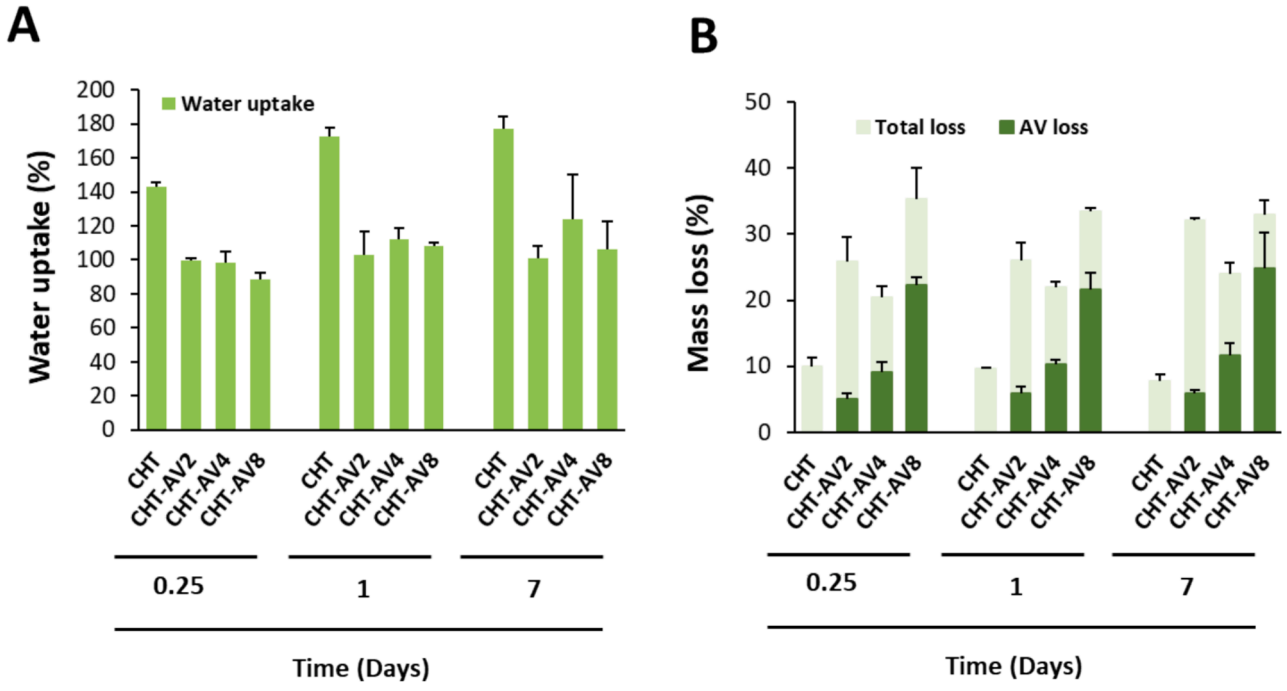

Fig. 5. Water uptake A) and mass loss B) of CHT and CHT-AV scaffold at 6 h, 1 and 7 days of incubation at 37 °C under orbital shaking (25 rpm). Mass loss includes total scaffold mass loss (light green) and AV-associated mass loss (dark green). n = 3.

incorporating amine functional nano-hydroxyapatite where the incorporation of this additional ingredient leads to a decrease in porosity together with a decrease in water uptake and swelling (Atak et al., 2017). Despite the higher initial mass loss of the scaffolds containing AV, no further changes could be observed in the integrity of the scaffolds at longer time points. A similar behavior was observed in our previous work for similar chitosan scaffolds showing a constant mass loss after the initial swelling for up to one month (Garcia-Garcia et al., 2021). This behavior would ensure the long-term stability of the systems, a critical point for their clinical application.

The scaffold morphology and the associated changes with AV incorporation was also evaluated using scanning electron microscopy as shown in Fig. 6. Scaffolds depicted a homogeneous microspheres dispersion within the chitosan and chitosan-AV structures (Fig. 6A-D). Moreover, after 7 days of swelling in water, the structure of the constructs was maintained (Fig. 6C-D). Scaffold porosity is a critical parameter that influences cell infiltration, nutrient diffusion, and tissue growth. High porosity values (80 %) are adequate to ensure suitable tissue integration and cell growth (Abbasi et al., 2020).

3.3. Evs loading and release profile

The EVs incorporation yield was 81.32 ± 5.31 %. Moreover, the EVs release from the scaffold occurred during the first 48 h showing a burst release of 42.22 ± 1.2 % within the first 2 h. After 12 h, 88.02 ± 3.27 % of the extracellular vesicles were released, and the release reached 94.87 ± 5.42 % at 24 h. This profile would be desirable to modulate the response of cells that migrate to the defect site after the scaffold implantation. Typically, EVs are incorporated within hydrogels. However, these systems require the use of cross-linkers that are usually added after the inclusion of EVs for hydrogel synthesis implying the risk of EVs integrity impairment (Hashemi et al., 2024). The elaborated systems overcome these disadvantages, since the cross-linker has already been removed from the system.

The bone regeneration process after hemostasis implies the recruitment and differentiation of stem cells that form skeletal and vascular tissues (Einhorn and Gerstenfeld, 2015).The initial interaction between the implanted biomaterials and the migrated cells will modulate the consequent healing cascade. In this sense, the initial cell microenvironment and adhesion is known to critically modulate cell differentiation and long-term biomaterial stability (Gao et al., 2017). Therefore, the developed EVs-loaded scaffolds could provide an adequate environment to the migrated stem cells inducing their proliferation and differentiation. The fast release observed for the EVs could be attributed to a neutralization of the chitosan charge associated to a basification of the media with the addition of PBS (pH 7.4) (Chang et al., 2020).

3.4. In vitro antibacterial activity

Histatin 5 is a cationic antimicrobial peptide naturally produced in saliva (Khan et al., 2013). Despite the proven antifungal and antibacterial activity, it has never been loaded in scaffolds for drug delivery. The antimicrobial activity of Hist-5 on *S. aureus* at concentrations ranging between 1.62 and 0.06 μg/μL was studied. The minimal inhibitory concentration (MIC) was established at 0.205 μg/μL. This concentration showed no bacterial growth after 24 h of treatment.

On the other hand, the antibacterial properties of aloe vera have been extensively exploited to develop systems for skin and bone regeneration (Alven et al., 2021; Shukla, 2022). The antibacterial properties of the developed CHT-AV scaffolds were studied using an agar diffusion assay (Fig. 7). CHT-AV2 and CHT-AV4 scaffolds showed significantly higher inhibitory halos than CHT scaffolds, only including

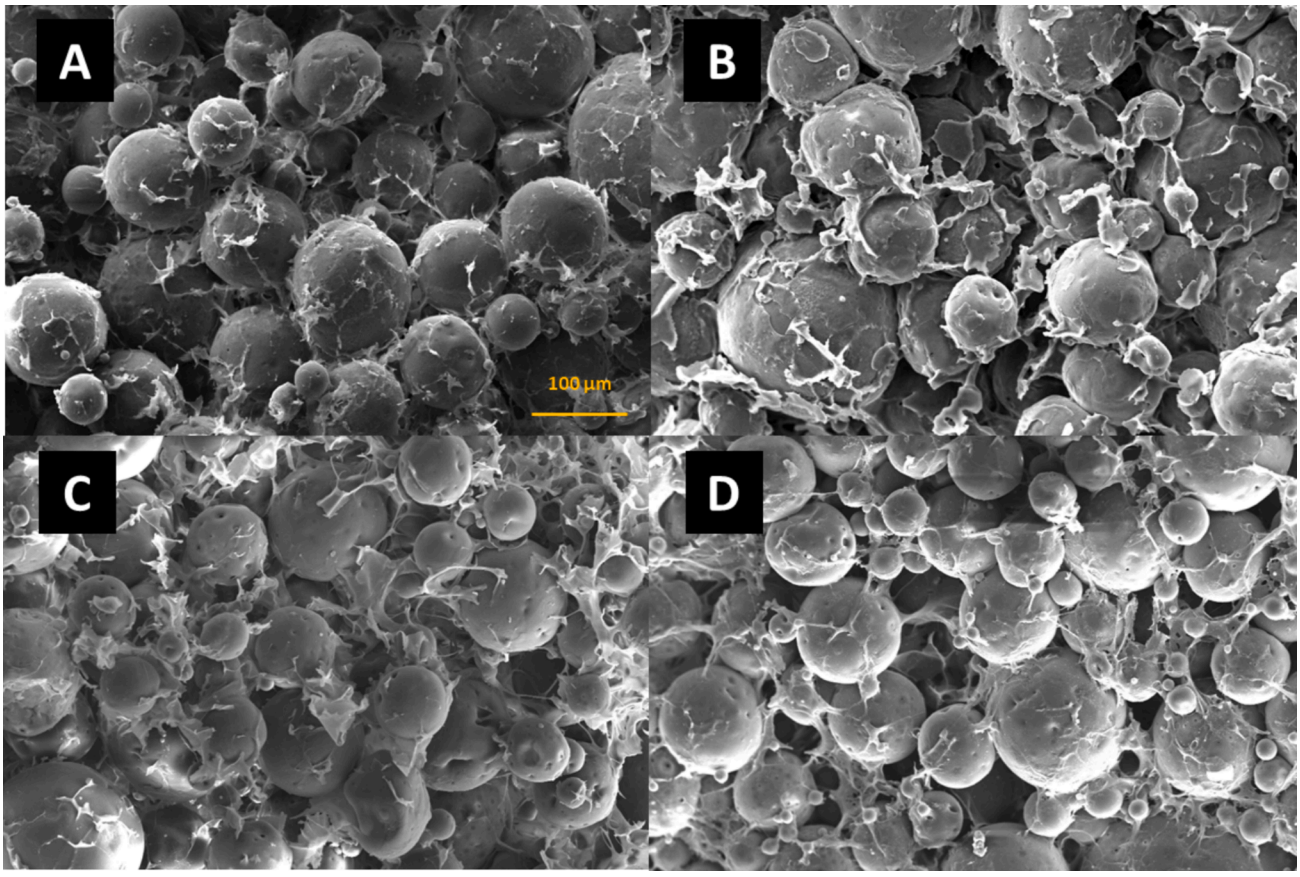

Fig. 6. Scanning electron microscopy images of A) freshly prepared chitosan scaffold; B) freshly prepared chitosan-aloe vera (CHT-AV2); C) chitosan scaffold after a 7 days incubation in water at 37 °C; D) CHT-AV2 scaffold after a 7 days incubation in water at 37 °C. (A-D): 160 X magnification.

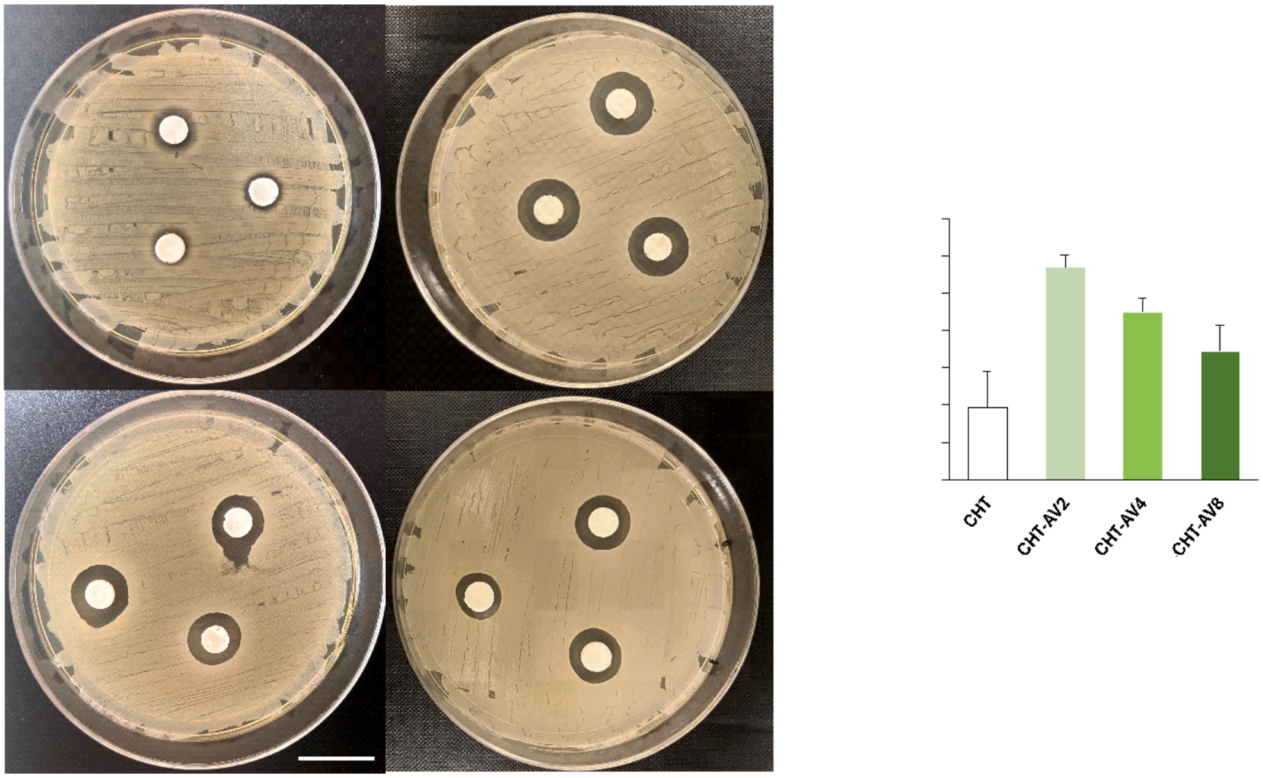

Fig. 7. In vitro antimicrobial assay against *S. aureus* of the obtained scaffolds. Images of A) CHT B) CHT- AV2 C) CHT-AV4 D) CHT-AV8 and E) Inhibition zone normalized width (nw) for the different scaffolds. (*) Denotes statistical differences to the CHT group. n = 3, scale bar = 20 mm.

chitosan. Contrary to expected, the scaffolds comprising the highest AV amount, CHT-AV8, produced lower inhibition for *Staphylococcus aureus* than CHT-AV2 and CHT-AV4. This effect could be related to the variation in the morphological and porous features of the scaffolds compared to systems containing less AV. These changes could hamper the AV diffusion from the scaffolds. Based on the results obtained, CHT-AV2 scaffolds were selected for the Amsterdam Active Attachment (AAA) biofilm assay model.

Staphylococcus aureus is present in 90 % of chronic osteomyelitis and can lead to tissue necrosis and the need for surgical intervention (Olson and Horswill, 2013). In addition, *S. aureus* can form biofilms in osteocyte lacunae hindering infection eradication (de Mesy Bentley et al., 2017).

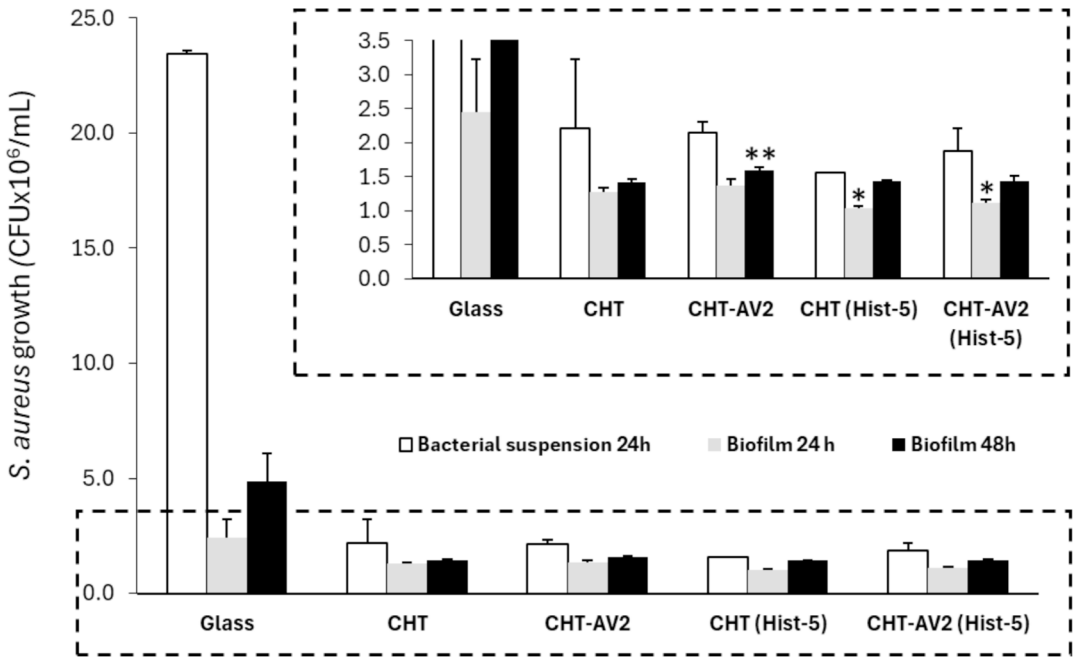

Fig. 8. A) *S. aureus* colony forming units (CFU) per mL of the bacterial suspension after 24 h of culture (white bars), and on the biofilm formed at 24 (grey bars) and 48 (black bars) hours. B) Enlargement of graph A (Dashed lines). (*) indicates statistically significant differences with the CHT group for biofilm at 24 h and (**) denotes statistical difference with the CHT group for biofilm at 48 h. n = 3, $p < 0.05$.

The capacity of the scaffolds to avoid the formation of the biofilm was evaluated using the AAA model. A piece of glass was used as positive control for the biofilm formation. Both the bacteria growing in the media as suspension and that incorporated within the biofilm network were quantified and shown in Fig. 8. In the glass control group, the bacteria present in the suspension was significantly higher compared to the initial concentration used for the experiment (8 ± 2.5 CFUx10^6/mL), with a value of 23.45 ± 0.12 CFU x10^6/mL. However, this behavior was different for the wells containing the scaffolds where the concentration of viable bacteria was lower than the initial one indicating a potent antibacterial activity of the scaffolds largely due to the antibacterial properties of CHT.

Despite the high concentration of the bacteria suspension for the glass control, the biofilm formed was limited, especially after 24 h of culture. However, the number of biofilm-forming bacteria increased significantly after 48 h (Fig. 8). The relatively low biofilm formation could be related to the composition of the media used for the experiment with low nutrient concentration as previous studies have reported that low glucose concentration conditions *S. aureus* biofilm formation (Silva et al., 2022).

Regarding the antibiofilm activity, scaffolds incorporating Hist-5 were able to significantly inhibit the formation of the biofilm after 24 h compared to control scaffolds (CHT). Moreover, no differences were observed between the systems prepared only with chitosan, CHT (Hist-5), or also including 2 mg of AV (CHT-AV2(Hist-5)). On the other hand, after 48 h, all the scaffolds showed significantly lower biofilm formation compared to the glass control.

The designed scaffolds were, therefore, suitable to avoid biofilm formation and designed to ensure a long-term antibacterial activity comprising the initial burst release of AV, afterwards the release of chitosan by degradation and, during the whole time the release of Hist-5 from the microspheres. Therefore, the CHT-AV scaffolds loaded with Hist-5 microspheres are a promising candidate for bone regeneration avoiding the risk of osteomyelitis.

3.5. Biological performance of the scaffolds

Fig. 9 shows the cell adhesion and proliferation of MSCs on the developed scaffolds. The incorporation of 2 mg of AV to chitosan scaffolds significantly improved cell adhesion and proliferation in the case of both unloaded and EVs-BMP-2-loaded systems. This effect was not observed for scaffolds with higher AV (4 and 8), probably due to the decreased scaffold porosity. This finding aligns with already published works that state a similar effect for chitosan membranes mixed with an aloe vera gel, showing an increased cell adhesion only at certain aloe vera gel concentrations (Silva et al., 2013).

Moreover, scaffolds incorporating 2 mg AV together with EV-BMP-2 showed the highest cell proliferation being 1.6-fold higher than that for the CHT control scaffolds. This effect could have been caused by the combination of EVs and AV. The beneficial effect on adhesion and proliferation of the incorporated MSCs-EVs in different scaffolds has been previously reported. As an example, Xing and coworkers developed electrospun silk fibroin/poly (ε-caprolactone) scaffold loaded with MSC-EVs that showed significantly enhanced cell migration and proliferation compared to the blank scaffolds (Xing et al., 2021). Another example is a β-tricalcium phosphate scaffolds loaded with human-induced pluripotent stem cell-derived mesenchymal stem cells EVs that showed enhanced proliferation, migration and osteogenic differentiation of MSCs, by activation of the PI3K/Akt pathway (Zhang et al., 2016).

The capacity of the scaffolds to finally induce the osteogenic differentiation of MSCs was evaluated at different timepoints by quantifying the number of alkaline phosphatase positive cells. This marker is a well-established method to identify early osteoblastic differentiation (Trivedi et al., 2020). The obtained results and representative images are shown in Fig. 10. For scaffolds not containing EVs, at the initial timepoint, in line with the adhesion and proliferation data, only scaffolds containing 2 mg of AV were able to significantly increase the number of ALP + cells compared to CHT. However, these differences were not observed after 21 days of culture.

Contrary, scaffolds incorporating EVs-BMP-2 showed an enhancement in ALP positive cells after 7 days in culture when AV was added at any of the concentrations used in the study. However, after 21 days of culture only CHT-AV2 and CHT-AV4 showed an enhanced osteogenic differentiation compared to CHT. This effect may be related to an enhancement in the basal number of ALP + cells in the control group (CHT) used for normalization. Interestingly, in these treatments the number of positive cells was 2-fold higher than the control. The beneficial effect of AV incorporation on ostogenesis and osteoinduction has been previously reported but limited to the toxicity of the obtained systems (Teymori et al., 2023). Moreover, it has been shown that EVs isolated from MSCs have the capacity to modify the bone regenerative response affecting osteogenesis and osteoclastogenesis. This

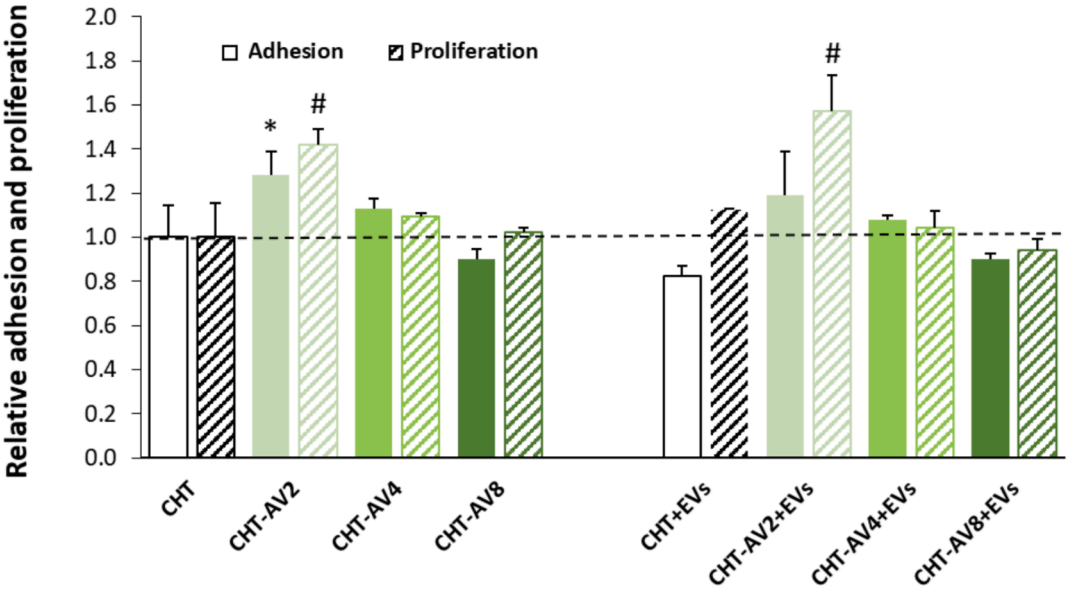

Fig. 9. MSCs adhesion (12 h) and proliferation (48 h) on CHT scaffolds with different aloe vera extract (AV) amounts without and with EVs (EVs-BMP2). (*) denotes statistically significant adhesion differences compared with CHT and (#) denotes statistical proliferation differences compared with CHT. $p < 0.05n = 3$.

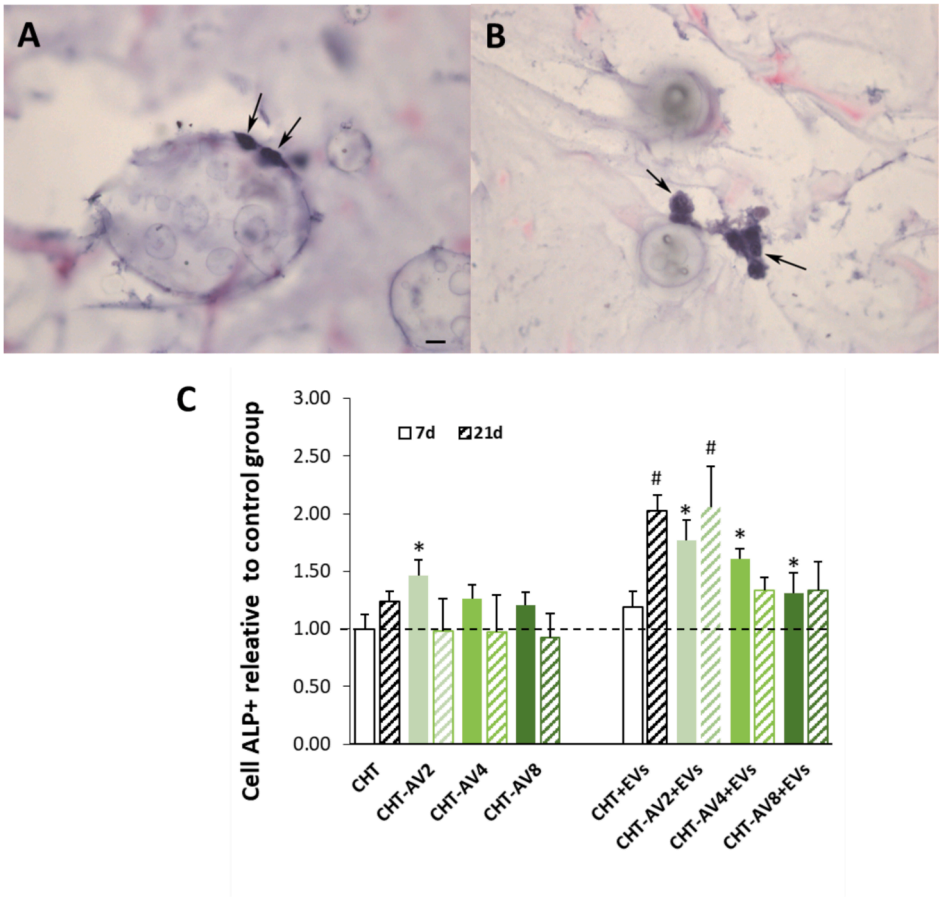

Fig. 10. Representative images of A) CHT scaffolds and B) CHT-AV2 stained with hematoxylin-erythrosine at 40X magnification. ALP + cells are indicated with a black arrow. C) ALP + cell quantification in CHT scaffolds with different aloe vera extract (AV) amounts without and with EVs (EVs-BMP-2) compared to the CHT control. (*) indicates statistically significant differences with the CHT at 7 days and (#) denotes statistical difference with CHT control group at 21 days. $p < 0.05n = 3$. Scale bar: 100 μm.

modification is highly correlated with the EVs cargo (Liu et al., 2023). In this work, MSCs were stimulated with several molecules and selected BMP-2 (200 ng/mL) as an adequate stimulus to produce EVs with a proliferative effect on MSCs while controlling fibroblasts proliferation. Huang and coworkers studied the osteogenic regenerative potential of EVs isolated from MSCs modified to constitutively express BMP-2 by lentiviral transfection. EVs isolated from these cells, despite not including BMP-2, enhanced the osteogenic capacity of MSCs and improved the regenerative response in a rat calvaria defect model (Huang et al., 2020). The osteogenic improvements were associated to an alteration in the miRNAs present in the vesicles that could potentially enhance the BMP-2 signaling cascade. Our results show a similar behavior for the isolated EVs-BMP-2 being able to induce the differentiation of MSCs towards osteoblasts.

The combination of EVs-BMP-2 with AV2 and Hist-5 in a CHT scaffold has been the most promising scaffold in terms of antibacterial properties, cell adhesion, proliferation and osteogenesis. This approach would avoid the biofilm formation on the implanted system without requiring the use of antibiotics while inducing the colonization of the biomaterials and the differentiation of cells.

These scaffolds would represent a breakthrough approach for enhancing bone regeneration and infection control for non-wear bearing applications in craniofacial reconstruction, dental bone grafting, segmental defect repair, and bone cyst treatment. These systems depict an acceptable scalability where the main limitation would be the isolation of EVs-BMP-2. The scaffolds containing Hist-5 could be obtained in a batch-based strategy by molding and, afterwards, the EVs can be added just before implantation. The large-scale production and isolation of EVs could be performed using bioreactor systems and size exclusion chromatography with automated sample collection. As a next step for the clinical translation, the bone regeneration capacity of CHT-AV2 scaffolds obtaining EVs-BMP-2 and Hist-5 are being evaluated in a mice model of bone defect.

Regarding the main limitations of the present study only a single dose of EVs has been used not allowing to optimize the dosing. Moreover, other EVs loading strategies could be developed to ensure a fast release profile is the adequate to obtain the desired osteogenic responses.

4. Conclusions

Tuned EVs were isolated by stimulating MSCs with different stimuli leading to the selection of EVs able to show different behavior on fibroblasts and MSCs. To the best of our knowledge, for the first time the antimicrobial peptide histatin-5 has been successfully encapsulated in microspheres. The obtained microspheres have been integrated within a chitosan and aloe vera matrix with physicochemical properties dependent on the amount of AV used. The use of 2 mg of AV has shown to be the best system with suitable antibacterial properties against *S. aureus*. Moreover, the additional incorporation of Hist-5 has led to scaffolds with both antibacterial and antibiofilm properties. Moreover, the addition of the selected EVs, EVs-BMP-2, together with the presence of AV improved the adhesion, proliferation and osteogenic differentiation of MSCs seeded on scaffolds. The combination of these therapeutic molecules allows in a single system to ensure infection inhibition and osteogenesis induction. However, further preclinical evaluation of the

scaffolds is required to assess the clinical translation of the developed scaffolds.

CRediT authorship contribution statement

Patricia García-García: Writing – original draft, Methodology, Investigation. **Carmen Évora:** Writing – review & editing, Resources, Conceptualization. **Araceli Delgado:** Writing – review & editing, Supervision, Project administration, Funding acquisition, Conceptualization. **Patricia Diaz-Rodriguez:** Writing – review & editing, Investigation, Data curation, Conceptualization.

Declaration of competing interest

The authors declare the following financial interests/personal relationships which may be considered as potential competing interests: [Araceli Delgado reports financial support was provided by Canarian Agency for Research Innovation and Information Society. Patricia Garcia-Garcia reports financial support was provided by University of La Laguna. If there are other authors, they declare that they have no known competing financial interests or personal relationships that could have appeared to influence the work reported in this paper].

Acknowledgments

This work was funded by ACIISI and FEDER "Canarias avanza con Europa" (ProID2020010086). P García-García acknowledges University of La Laguna for the action: "Recualificación de personal Universitario: Margarita Salas para la formación de jóvenes doctores".

Data availability

Data will be made available on request.

References

Abbasi, N., Hamlet, S., Love, R.M., Nguyen, N.-T., 2020. Porous scaffolds for bone regeneration. J. Sci.: Adv. Mater. Devices 5, 1–9.
Alven, S., Khwaza, V., Oyedeji, O.O., Aderibigbe, B.A., 2021. Polymer-based scaffolds loaded with aloe vera extract for the treatment of wounds. Pharmaceutics 13.
Aranaz, I., Alcantara, A.R., Civera, M.C., Arias, C., Elorza, B., Heras Caballero, A., Acosta, N., 2021. Chitosan: an overview of its properties and applications. Polymers 13.
Atak, B.H., Buyuk, B., Huysal, M., Isik, S., Senel, M., Metzger, W., Cetin, G., 2017. Preparation and characterization of amine functional nano-hydroxyapatite/chitosan bionanocomposite for bone tissue engineering applications. Carbohydr. Polym. 164, 200–213.
Bhakta, G., Rai, B., Lim, Z.X., Hui, J.H., Stein, G.S., van Wijnen, A.J., Nurcombe, V., Prestwich, G.D., Cool, S.M., 2012. Hyaluronic acid-based hydrogels functionalized with heparin that support controlled release of bioactive BMP-2. Biomaterials 33, 6113–6122.
Boparai, J.K., Sharma, P.K., 2020. Mini review on antimicrobial peptides, sources, mechanism and recent applications. Protein Pept. Lett. 27, 4–16.
Bouchareychas, L., Duong, P., Covarrubias, S., Alsop, E., Phu, T.A., Chung, A., Gomes, M., Wong, D., Meechoovet, B., Capili, A., Yamamoto, R., Nakauchi, H., McManus, M.T., Carpenter, S., Van Keuren-Jensen, K., Raffai, R.L., 2020. Macrophage exosomes resolve atherosclerosis by regulating hematopoiesis and inflammation via MicroRNA cargo. Cell Rep. 32, 107881.
Briffault, E., Garcia-Garcia, P., Martinez-Borrajo, R., Evora, C., Delgado, A., Diaz-Rodriguez, P., 2024. Harnessing extracellular vesicle membrane for gene therapy: EVs-biomimetic nanoparticles. Colloids Surf. BBiointerfaces 239, 113951.
Chang, H.-H., Cheng, N.-C., Ethan Li, Y.-C., Wang, J.-H., Young, T.-H., 2020. pH-responsive characteristics of chitosan-based blends for controlling the adhesivity of cells. J. Taiwan Inst. Chem. Eng. 111, 34–43.
Chen, S., Sun, F., Qian, H., Xu, W., Jiang, J., 2022. Preconditioning and engineering strategies for improving the efficacy of mesenchymal stem cell-derived exosomes in cell-free therapy. Stem Cells Int. 2022, 1779346.
de Mesy Bentley, K.L., Trombetta, R., Nishitani, K., Bello-Irizarry, S.N., Ninomiya, M., Zhang, L., Chung, H.L., McGrath, J.L., Daiss, J.L., Awad, H.A., Kates, S.L., Schwarz, E.M., 2017. Evidence of staphylococcus aureus deformation, proliferation, and migration in canaliculi of live cortical bone in murine models of osteomyelitis. J. Bone Miner. Res. Off. J. Am. Soc. Bone Miner. Res. 32, 985–990.
De Oliveira, D.M.P., Forde, B.M., Kidd, T.J., Harris, P.N.A., Schembri, M.A., Beatson, S. A., Paterson, D.L., Walker, M.J., 2020. Antimicrobial Resistance in ESKAPE Pathogens. Clinical microbiology reviews 33.
Del Rosario, C., Rodriguez-Evora, M., Reyes, R., Simoes, S., Concheiro, A., Evora, C., Alvarez-Lorenzo, C., Delgado, A., 2015. Bone critical defect repair with poloxamine-cyclodextrin supramolecular gels. Int. J. Pharm. 495, 463–473.
Du, H., Puri, S., McCall, A., Norris, H.L., Russo, T., Edgerton, M., 2017. Human salivary protein histatin 5 has potent bactericidal activity against ESKAPE pathogens. Front. Cell. Infect. Microbiol. 7, 41.
Einhorn, T.A., Gerstenfeld, L.C., 2015. Fracture healing: mechanisms and interventions. Nat. Rev. Rheumatol. 11, 45–54.
Fu, L., Tang, T., Miao, Y., Zhang, S., Qu, Z., Dai, K., 2008. Stimulation of osteogenic differentiation and inhibition of adipogenic differentiation in bone marrow stromal cells by alendronate via ERK and JNK activation. Bone 43, 40–47.
Gao, C., Peng, S., Feng, P., Shuai, C., 2017. Bone biomaterials and interactions with stem cells. Bone Res. 5, 17059.
Gao, M., Gao, W., Papadimitriou, J.M., Zhang, C., Gao, J., Zheng, M., 2018. Exosomes-the enigmatic regulators of bone homeostasis. Bone Res. 6, 36.
Garcia-Garcia, P., Reyes, R., Rodriguez, J.A., Martin, T., Evora, C., Diaz-Rodriguez, P., Delgado, A., 2021. The bone regeneration capacity of BMP-2 + MMP-10 loaded scaffolds depends on the tissue status. Pharmaceutics 13.
Garcia-Garcia, P., Reyes, R., Segredo-Morales, E., Perez-Herrero, E., Delgado, A., Evora, C., 2019. PLGA-BMP-2 and PLA-17beta-estradiol microspheres reinforcing a composite hydrogel for bone regeneration in osteoporosis. Pharmaceutics 11.
Gomez Chabala, L.F., Cuartas, C.E.E., Lopez, M.E.L., 2017. Release Behavior and Antibacterial Activity of Chitosan/Alginate Blends with Aloe vera and Silver Nanoparticles. Marine drugs 15.
Gul, B., Syed, F., Khan, S., Iqbal, A., Ahmad, I., 2022. Characterization of extracellular vesicles by flow cytometry: challenges and promises. Micron 161, 103341.
Habeeb, F., Shakir, E., Bradbury, F., Cameron, P., Taravati, M.R., Drummond, A.J., Gray, A.I., Ferro, V.A., 2007. Screening methods used to determine the anti-microbial properties of Aloe vera inner gel. Methods 42, 315–320.
Hahm, J., Kim, J., Park, J., 2021. Strategies to enhance extracellular vesicle production. Tissue Eng. Regener. Med. 18, 513–524.
Hamman, J.H., 2008. Composition and applications of Aloe vera leaf gel. Molecules 13, 1599–1616.
Hashemi, A., Ezati, M., Nasr, M.P., Zumberg, I., Provaznik, V., 2024. Extracellular vesicles and hydrogels: an innovative approach to tissue regeneration. ACS Omega 9, 6184–6218.
Hashemi, S.A., Madani, S.A., Abediankenari, S., 2015. The review on properties of aloe vera in healing of cutaneous wounds. Bio. Med. Res. Int. 2015, 714216.
He, Y., Wang, Y., Yu, S., Wang, L., Dou, Y., Ma, R., Cao, S., Song, W., Ma, P., 2024. BMP2 enhance the osteogenic effect of BMSCs-derived exosomes in skull defect of diabetic rats. Mater. Des. 248, 113517.
Huang, C.C., Kang, M., Lu, Y., Shirazi, S., Diaz, J.I., Cooper, L.F., Gajendrareddy, P., Ravindran, S., 2020. Functionally engineered extracellular vesicles improve bone regeneration. Acta Biomaterialia 109, 182–194.
Jaiswal, N., Haynesworth, S.E., Caplan, A.I., Bruder, S.P., 1997. Osteogenic differentiation of purified, culture-expanded human mesenchymal stem cells in vitro. J. Cell. Biochem. 64, 295–312.
Jensen, L.K., Koch, J., Aalbaek, B., Moodley, A., Bjarnsholt, T., Kragh, K.N., Petersen, A., Jensen, H.E., 2017. Early implant-associated osteomyelitis results in a peri-implanted bacterial reservoir. APMIS Acta Pathologica, Microbiologica, et Immunologica Scandinavica 125, 38–45.
Ji, J.F., He, B.P., Dheen, S.T., Tay, S.S., 2004. Interactions of chemokines and chemokine receptors mediate the migration of mesenchymal stem cells to the impaired site in the brain after hypoglossal nerve injury. Stem Cells 22, 415–427.
Khan, S.A., Fidel Jr., P.L., Thunayyan, A.A., Varlotta, S., Meiller, T.F., Jabra-Rizk, M.A., 2013. Impaired histatin-5 levels and salivary antimicrobial activity against C. albicans in HIV infected individuals. J. AIDS & Clin. Res. 4.
Koritzinsky, E.H., Street, J.M., Star, R.A., Yuen, P.S., 2017. Quantification of exosomes. J. Cell. Physiol. 232, 1587–1590.
Kou, M., Huang, L., Yang, J., Chiang, Z., Chen, S., Liu, J., Guo, L., Zhang, X., Zhou, X., Xu, X., Yan, X., Wang, Y., Zhang, J., Xu, A., Tse, H.-F., Lian, Q., 2022. Mesenchymal stem cell-derived extracellular vesicles for immunomodulation and regeneration: a next generation therapeutic tool? Cell Death Dis. 13, 580.
Kremers, H.M., Nwojo, M.E., Ransom, J.E., Wood-Wentz, C.M., Melton 3rd, L.J., Huddleston 3rd, P.M., 2015. Trends in the epidemiology of osteomyelitis: a population-based study, 1969 to 2009. J. Bone Joint Surg. Am. 97, 837–845.
Liu, R., Wu, S., Liu, W., Wang, L., Dong, M., Niu, W., 2023. microRNAs delivered by small extracellular vesicles in MSCs as an emerging tool for bone regeneration. Front. Bioeng. Biotechnol. 11, 1249860.
Liu, Y.S., Ou, M.E., Liu, H., Gu, M., Lv, L.W., Fan, C., Chen, T., Zhao, X.H., Jin, C.Y., Zhang, X., Ding, Y., Zhou, Y.S., 2014. The effect of simvastatin on chemotactic capability of SDF-1alpha and the promotion of bone regeneration. Biomaterials 35, 4489–4498.
Lopes, R., Gordo, P.M., Costa, B.F.O., Alves, P., 2024. Formulation and characterization of chitosan-based mixed-matrix scaffold for tissue engineering. Macromol 253–268.
Lu, J., Yang, X., He, C., Chen, Y., Li, C., Li, S., Chen, Y., Wu, Y., Xiang, Z., Kang, J., Jiang, G., Wang, C., Diarra, M.D., He, R., Feng, G., Yan, R., 2023. Rejuvenation of tendon stem/progenitor cells for functional tendon regeneration through platelet-derived exosomes loaded with recombinant Yap1. Acta Biomaterialia 161, 80–99.
Man, K., Brunet, M.Y., Federici, A.S., Hoey, D.A., Cox, S.C., 2022. An ECM-mimetic hydrogel to promote the therapeutic efficacy of osteoblast-derived extracellular vesicles for bone regeneration. Front. Bioeng. Biotechnol. 10, 829969.
Man, K., Eisenstein, N.M., Hoey, D.A., Cox, S.C., 2023. Bioengineering extracellular vesicles: smart nanomaterials for bone regeneration. J. Nanobiotechnol. 21, 137.
Marti, M., Frigols, B., Serrano-Aroca, A., 2018. Antimicrobial characterization of advanced materials for bioengineering applications. J. Visualized Exp.: JoVE.

Martinez-Borrajo, R., Diaz-Rodriguez, P., Landin, M., 2023. Rationalized design to explore the full potential of PLGA microspheres as drug delivery systems. Drug Deliv. 30, 2219864.
Mehrvar, A., Akbari, M., Khosroshahi, E.M., Nekavand, M., Mokhtari, K., Baniasadi, M., Aghababaian, M., Karimi, M., Amiri, S., Moazen, A., Maghsoudloo, M., Alimohammadi, M., Rahimzadeh, P., Farahani, N., Vaghar, M.E., Entezari, M., Hashemi, M., 2024. The impact of exosomes on bone health: a focus on osteoporosis. Pathol. Res. Pract. 263, 155618.
Moormeier, D.E., Bayles, K.W., 2017. Staphylococcus aureus biofilm: a complex developmental organism. Mol. Microbiol. 104, 365–376.
O'Donnell, P.B., McGinity, J.W., 1997. Preparation of microspheres by the solvent evaporation technique. Adv. Drug Deliv. Rev. 28, 25–42.
Olson, M.E., Horswill, A.R., 2013. Staphylococcus aureus osteomyelitis: bad to the bone. Cell Host Microbe 13, 629–631.
Pakshir, P., Hinz, B., 2018. The big five in fibrosis: Macrophages, myofibroblasts, matrix, mechanics, and miscommunication. MatrixBiol.: J. Int. Soc. Matrix Biol. 68–69, 81–93.
Palmieri, V., Lucchetti, D., Gatto, I., Maiorana, A., Marcantoni, M., Maulucci, G., Papi, M., Pola, R., De Spirito, M., Sgambato, A., 2014. Dynamic light scattering for the characterization and counting of extracellular vesicles: a powerful noninvasive tool. J. Nanopart. Res. 16, 2583.
Pape, H.C., Evans, A., Kobbe, P., 2010. Autologous bone graft: properties and techniques. J. Orthop. Trauma 24 (Suppl 1), S36–S40.
Radha, M.H., Laxmipriya, N.P., 2015. Evaluation of biological properties and clinical effectiveness of Aloe vera: a systematic review. J. Tradit. Complement. Med. 5, 21–26.
Radomsky, M.L., Thompson, A.Y., Spiro, R.C., Poser, J.W., 1998. Potential role of fibroblast growth factor in enhancement of fracture healing. Clin. Orthop. Relat. Res. S283–S293.
Ren, J., Yu, R., Xue, J., Tang, Y., Su, S., Liao, C., Guo, Q., Guo, W., Zheng, J., 2022. How do extracellular vesicles play a key role in the maintenance of bone homeostasis and regeneration? A comprehensive review of literature. Int. J. Nanomed. 17, 5375–5389.
Reyes, R., De la Riva, B., Delgado, A., Hernandez, A., Sanchez, E., Evora, C., 2012. Effect of triple growth factor controlled delivery by a brushite-PLGA system on a bone defect. Injury 43, 334–342.
Shao, J., Zhu, J., Chen, Y., Fu, Q., Li, L., Ding, Z., Wu, J., Han, Y., Li, H., Qian, Q., Zhou, Y., 2021. Exosomes from Kartogenin-Pretreated infrapatellar fat pad mesenchymal stem cells enhance chondrocyte anabolism and articular cartilage regeneration. Stem Cells Int. 2021, 6624874.
Shea, C.M., Edgar, C.M., Einhorn, T.A., Gerstenfeld, L.C., 2003. BMP treatment of C3H10T1/2 mesenchymal stem cells induces both chondrogenesis and osteogenesis. J. Cell. Biochem. 90, 1112–1127.
Shiels, S.M., Bedigrew, K.M., Wenke, J.C., 2015. Development of a hematogenous implant-related infection in a rat model. BMC Musculoskelet. Disord. 16, 255.
Shukla, D.G., S.B., Bandyopadhyay-Ghosh, S.; Mishra D., 2022. Aloe-vera-based biopolymeric composite scaffolds for bone tissue engineering: a review. Mater. Today Proc. 79.
Silva, S.S., Caridade, S.G., Mano, J.F., Reis, R.L., 2013. Effect of crosslinking in chitosan/aloe vera-based membranes for biomedical applications. Carbohydr. Polym. 98, 581–588.
Silva, V., Pereira, J.E., Maltez, L., Poeta, P., Igrejas, G., 2022. Influence of environmental factors on biofilm formation of staphylococci isolated from wastewater and surface water, Pathogens.
Tang, J., Wang, X., Lin, X., Wu, C., 2024. Mesenchymal stem cell-derived extracellular vesicles: a regulator and carrier for targeting bone-related diseases. Cell Death Discovery 10, 212.
Tarin-Pello, A., Suay-Garcia, B., Perez-Gracia, M.T., 2022. Antibiotic resistant bacteria: current situation and treatment options to accelerate the development of a new antimicrobial arsenal. Expert Rev. Anti Infect. Ther. 20, 1095–1108.
Teymori, M., Karimi, E., Saburi, E., 2023. Evaluation of osteoconductive effect of polycaprolactone (PCL) scaffold treated with Aloe vera on adipose-derived mesenchymal stem cells (ADSCs). Am. J. Stem Cells 12, 83–91.
Trivedi, S., Srivastava, K., Gupta, A., Saluja, T.S., Kumar, S., Mehrotra, D., Singh, S.K., 2020. A quantitative method to determine osteogenic differentiation aptness of scaffold. J. Oral Biol. Craniofacial Res. 10, 158–160.
Vergauwen, G., Dhondt, B., Van Deun, J., De Smedt, E., Berx, G., Timmerman, E., Gevaert, K., Miinalainen, I., Cocquyt, V., Braems, G., Van den Broecke, R., Denys, H., De Wever, O., Hendrix, A., 2017. Confounding factors of ultrafiltration and protein analysis in extracellular vesicle research. Sci. Rep. 7, 2704.
Vivero-Lopez, M., Xu, X., Muras, A., Otero, A., Concheiro, A., Gaisford, S., Basit, A.W., Alvarez-Lorenzo, C., Goyanes, A., 2021. Anti-biofilm multi drug-loaded 3D printed hearing aids. Korean J. Couns. Psychother. 119, 111606.
Wan, Y., Fang, Y., Wu, H., Cao, X., 2007. Porous polylactide/chitosan scaffolds for tissue engineering. J. Biomed. Mater. Res. A 80, 776–789.
Wang, L., Jia, Y., Wu, J., Cai, Y., Guo, Q., Sun, W., Zhang, Y., Mason, C.E., Shi, T., 2023. The effect of greenness on ESKAPE pathogen reduction and its heterogeneity across global climate zones and urbanization gradient. Urban Urban Gree. 87, 128048.
Xing, X., Han, S., Ni, Y., Cheng, G., Cheng, Y., Ni, X., Deng, Y., Li, Z., Li, Z., 2021. Mussel-inspired functionalization of electrospun scaffolds with polydopamine-assisted immobilization of mesenchymal stem cells-derived small extracellular vesicles for enhanced bone regeneration. Int. J. Pharm. 609, 121136.
Yang, S., Zhu, B., Yin, P., Zhao, L., Wang, Y., Fu, Z., Dang, R., Xu, J., Zhang, J., Wen, N., 2020. Integration of human umbilical cord mesenchymal stem cells-derived exosomes with hydroxyapatite-embedded hyaluronic acid-alginate hydrogel for bone regeneration. ACS Biomater Sci. Eng. 6, 1590–1602.
Youseflee, P., Ranjbar, F.E., Bahraminasab, M., Ghanbari, A., Faradonbeh, D.R., Arab, S., Alizadeh, A., Nooshabadi, V.T., 2023. Exosome loaded hydroxyapatite (HA) scaffold promotes bone regeneration in calvarial defect: an in vivo study. Cell Tissue Bank. 24, 389–400.
Yu, M., Liu, W., Li, J., Lu, J., Lu, H., Jia, W., Liu, F., 2020. Exosomes derived from atorvastatin-pretreated MSC accelerate diabetic wound repair by enhancing angiogenesis via AKT/eNOS pathway. Stem Cell Res Ther 11, 350.
Zhang, E., Miramini, S., Zhang, L., 2024. The impact of osteoporosis and diabetes on fracture healing under different loading conditions. Comput. Methods Programs Biomed. 244, 107952.
Zhang, J., Liu, X., Li, H., Chen, C., Hu, B., Niu, X., Li, Q., Zhao, B., Xie, Z., Wang, Y., 2016. Exosomes/tricalcium phosphate combination scaffolds can enhance bone regeneration by activating the PI3K/Akt signaling pathway. Stem Cell Res Ther 7, 136.
Zhang, K., Zhao, X., Chen, X., Wei, Y., Du, W., Wang, Y., Liu, L., Zhao, W., Han, Z., Kong, D., Zhao, Q., Guo, Z., Han, Z., Liu, N., Ma, F., Li, Z., 2018. Enhanced therapeutic effects of mesenchymal stem cell-derived exosomes with an injectable hydrogel for hindlimb ischemia treatment. ACS Appl. Mater. Interfaces 10, 30081–30091.
Zheng, P., Chen, L., Yuan, X., Luo, Q., Liu, Y., Xie, G., Ma, Y., Shen, L., 2017. Exosomal transfer of tumor-associated macrophage-derived miR-21 confers cisplatin resistance in gastric cancer cells. J. Exp. Clin. Cancer Res.: CR 36, 53.